Characterization of the Sol−Gel Formation of Iron(III) Oxide/Hydroxide Nanonetworks from Weak Base Molecules

Jeremy D. Walker and Rina Tannenbaum*

School of Materials Science and Engineering, Georgia Institute of Technology, Atlanta, Georgia 30332

Received April 20, 2006. Revised Manuscript Received July 18, 2006

This work deals with the synthesis of iron(III) oxide/hydroxide xerogels from a hydrated ferric nitrate precursor salt ($Fe(NO_3)_3 \cdot 9H_2O$) through the addition of different weak base chemicals (e.g., propylene oxide, pyridine, and tetrahydrofuran) as gelation agents. The dried xerogel samples were characterized by X-ray photoelectron spectroscopy (XPS), X-ray diffraction (XRD), transmission electron microscopy (TEM), and atomic force microscopy (AFM). XPS and XRD data show $Fe(2p_{3/2})$ and $Fe(2p_{1/2})$ peaks at values corresponding to that of an amorphous Fe_2O_3/FeO(OH) material. The morphology of the iron oxide/hydroxide xerogels obtained from TEM and AFM images indicates the formation of a "nanonetwork" assembly, with base particles of ∼5 nm in diameter aggregated into a network of clusters ∼30 nm in size. In addition to sample characterization, a mechanistic study was performed to probe the formation of the iron oxide/hydroxide xerogel using the three different weak base gelation agents. Previous work, in which propylene oxide was used as the gelation agent, has proposed that a "proton scavenging" mechanism was responsible for the formation of the xerogel. In the current study, this mechanistic view has been further investigated and generalized to encompass a broader class of weak bases through pH studies, XPS, and infrared spectroscopy.

Introduction

The synthesis of metal oxides by sol−gel synthesis has proven extremely versatile since it allows the formation of a large variety of metal oxides at relatively low temperatures via the processing of metal salt or metal alkoxide precursors.[1] These oxides may be used in a variety of applications in the areas of sensors, optical materials, catalysts, gas separation, information storage, wet-type solar cells, oxide ion conductors for solid-oxide fuel cells, and many other research areas.[2−19] Specifically, iron(III) oxides formed by sol−gel synthesis have been extensively studied for their use as sensors, as catalysts, and as magnetic recording media.[20−26]

Previous research has demonstrated that iron(III) oxides formed via the sol−gel process from iron salt precursors in the presence of epoxides[27] possess properties such as high porosity, high surface area, and low density.[28,29] Our interest in exploiting these properties lies in the design of metal oxide matrices for energetic materials. These materials are comprised of a particulate metal fuel (e.g., Al, Fe, Cr) closely mixed with metal oxide particles, which, after a stress-induced oxidation−reduction reaction, result in a substantial exothermic heat release (for example, see Arnáiz et al. in ref 17). In these materials, reactions between different metal oxide networks (oxidants) and dispersed metallic particles (fuels) will result in different energetic release rates, as shown in the following typical exothermic reaction:

$$Fe_2O_3 + 2Al \xrightarrow{\text{stress}} 2Fe + Al_2O_3 + \Delta H_R\left(\frac{-852\ \text{kJ}}{\text{mol}}\right) \quad (1)$$

An important parameter governing the efficiency of the energetic output of the reaction is the interfacial area and

* Corresponding author. E-mail: rina.tannenbaum@mse.gatech.edu.

(1) Battisha, I. K.; Afify, H. H.; Hamada, I. M. *J. Magn. Magn. Mater.* **2005**, *292*, 440.
(2) Aitasalo, T.; Holsa, J.; Jungner, H.; Lastusaari, M.; Niittykoski, J.; Saarinen, J. *Opt. Mater.* **2005**, *27* (9), 1537.
(3) Baiju, K. V.; Sibu, C. P.; Rajesh, K.; Pillai, P. K.; Mukundan, P.; Warrier, K. G. K.; Wunderlich, W. *Mater. Chem. Phys.* **2005**, *90* (1), 123.
(4) Celerier, S.; Laberty-Robert, C.; Ansart, F.; Calmet, C.; Stevens, P. *J. Eur. Ceram. Soc.* **2005**, *25* (12), 2665.
(5) Fu, L. J.; Liu, H.; Li, C.; Wu, Y. P.; Rahm, E.; Holze, R.; Wu, H. Q. *Prog. Mater. Sci.* **2005**, *50* (7), 881.
(6) Garcia Cerda, L. A.; Montemayor, S. M. *J. Magn. Magn. Mater.* **2005**, *294* (2), e43.
(7) Houbertz, R. *Appl. Surf. Sci.* **2005**, *247* (1−4), 504.
(8) Hsiao, C. N.; Huang, K. S. *J. Appl. Polym. Sci.* **2005**, *96* (5), 1936−1942.
(9) Huang, X. H.; Chen, Z. H. *J. Cryst. Growth* **2004**, *271*, 287−293.
(10) Jan, S.-S.; Chen, Y.-C.; Chou, J.-C. *Sens. Actuators B* **2005**, *108* (1−2), 883.
(11) Kiisk, V.; Sildos, I.; Lange, S.; Reedo, V.; Tatte, T.; Kirm, M.; Aarik, J. *Appl. Surf. Sci.* **2005**, *247* (1−4), 412.
(12) Mao, L.; Li, Q.; Dang, H.; Zhang, Z. *Mater. Res. Bull.* **2005**, *40* (2), 201.
(13) Moussa, N.; Ghorbel, A.; Grange, P. *J. Sol−Gel Sci. Technol.* **2005**, *33* (1), 127−132.
(14) Pustelny, T.; Zielonka, I.; Karasinski, P.; Jurusik, J. *Opt. Appl.* **2004**, *34* (4), 477−487.
(15) Ristic, M.; Popovic, S.; Music, S. *Mater. Lett.* **2005**, *59* (10), 1227.
(16) Xomeritakis, G.; Tsai, C.-Y.; Brinker, C. J. *Sep. Purif. Technol.* **2005**, *42* (3), 249.
(17) Arnáiz, F. J.; Aguado, R.; Arnáiz, S. *J. Chem. Educ.* **1998**, *75*, 1630.
(18) Huang, X.-H.; Chen, Z.-H. *Solid State Commun.* **2004**, *132* (12), 845.
(19) Miyake, H.; Kozuka, H. *J. Phys. Chem. B* **2005**, *109*, 17951−17956.
(20) Eerenstein, W.; Kalev, L.; Niesen, L.; Palstra, T. T. M.; Hibma, T. *J. Magn. Magn. Mater.* **2003**, *258*, 73.
(21) Fabrizoli, P.; Burgi, T.; Baiker, A. *J. Catal.* **2002**, *206*, 143−154.
(22) Pajonk, G. M. *Catal. Today* **1997**, *35* (3), 319.
(23) Tongpool, R.; Jindasuwan, S. *Sens. Actuators B* **2005**, *106* (2), 523−528.
(24) Wang, C.-T.; Ro, S.-H. *Appl. Catal. A* **2005**, *285* (1-2), 196.
(25) Long, J. W.; Logan, M. S.; Rhodes, C. P.; Carpenter, E. E.; Stroud, R. M.; Rolison, D. R. *J. Am. Chem. Soc.* **2004**, *126* (51), 16879−16889.
(26) Lin, Y.; Sun, F. Q.; Yuan, X. Y.; Geng, B. Y.; Zhang, L. D. *Appl. Phys. A: Mater. Sci. Process* **2004**, *78* (8), 1197.
(27) Gash, A. E.; Tillotson, T. M.; Jr., J. H. S.; Poco, J. F.; Hrubesh, L. W.; Simpson, R. L. *Chem. Mater.* **2001**, *13* (3), 999−1007.
(28) Gash, A. E.; Satcher, J. H. J.; Simpson, R. L. *Chem. Mater.* **2003**, *15*, 3268−3275.

10.1021/cm0609101 CCC: $33.50
Published on Web 09/07/2006

the reactivity between the metal fuel and the metal oxide particles. Clearly, reducing the size of the metal oxide (oxidant) netwok as well as the size of the particulate metal fuel to the nanometer scale will dramatically increase the interfacial area and will directly translate into a higher efficiency of the oxidation−reduction reaction. One way to accomplish this is to modify the original sol−gel reaction by introducing different types of gelation agents, which will allow for a higher degree of control over the gelation step and promote the formation of nanoscale metal oxide networks (i.e., nanonetworks),

The general mechanistic view regarding the formation of the Fe_2O_3 xerogel by the addition of an epoxide to a hydrated iron nitrate solution is based on the assumption that the gelation agent, propylene oxide (a 1,2-epoxide), can be regarded as a weak base that does not cause vigorous precipitation of Fe^{III}. The use of a weak base is emphasized as strong bases are known to form iron oxide precipitates due to the rapid reaction rate of the base with the metal species.[30] Propylene oxide has traditionally been used in organic syntheses as an acid scavenger.[31] In this scenario, the propylene oxide acts as a "proton scavenger" extracting protons from the water molecules in the immediate coordination sphere of the hydrated metal complex, resulting in a protonated epoxide. The protonated epoxide subsequently undergoes irreversible ring-opening by reacting with a nucleophile present in solution, either a nitrate ion or water. Then, as a result of this ring-opening reaction in which a protonated diol is formed, deprotonation occurs and a diol is formed in conjunction with a net elimination of protons from solution. After further hydrolysis and condensation of the original hydrated metal complex and increased heating, stoichiometric Fe_2O_3 is formed. This series of events is shown in eqs 2 and 3.

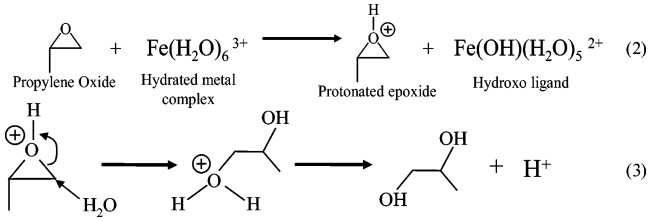

This proposed mechanism was validated by the researchers through pH and NMR studies.[27]

The work presented in this paper is concerned with an extension and generalization of the synthesis of iron(III) oxides achieved by the addition of a weak base to hydrated iron nitrate precursor solutions. By performing the synthesis according to the same general procedure based on the reaction of a hydrated iron salt dissolved in ethanol, the effect of the addition of other weak base gelation chemicals will be studied. In addition to adding propylene oxide (a 1,2-epoxide) as the gelation chemical, other weak bases, such as 1,4-epoxide, tetrahydrofuran, and pyridine (a heterocyclic nitrogen-containing compound) are studied. Figure 1 shows the chemical structure of these chemicals.

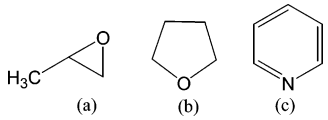

Figure 1. Structures of weak base molecules: (a) propylene oxide, a 1,2-epoxide; (b) tetrahydrofuran, a 1,4-epoxide; and (c) pyridine.

Characterization of the synthesized iron(III) oxide materials will be accomplished through X-ray photoelectron spectroscopy (XPS), X-ray diffraction (XRD), transmission electron microscopy (TEM), and atomic force microscopy (AFM). In addition to characterization of the synthesized materials, reaction mechanisms for the different systems are proposed from supporting pH studies during the sol to gel transformation as well as Fourier-transform infrared (FTIR) spectroscopy and XPS measurements.

Experimental Section

Synthesis of Iron(III) Oxide Xerogels. Ferric nitrate nonahydrate, $Fe(NO_3)_3 \cdot 9H_2O$; tetrahydrofuran (THF), C_4H_8O; pyridine, C_5H_5N; and propylene oxide, C_3H_6O, were purchased from Fisher Scientific and used as received. Stock absolute ethanol was also obtained and used as received. Syntheses were performed in 20 mL glass scintillation vials and performed under ambient conditions. For all syntheses, 0.65 g of $Fe(NO_3)_3 \cdot 9H_2O$ was added to 3.5 mL of ethanol and stirred until the solid ferric nitrate component was completely dissolved in the ethanol. Then a 1.2 mL allotment of weak base, propylene oxide, THF, or pyridine, was added as the gelation chemical to the solution and stirred. After addition of the gelation chemical, times to gelation were monitored and recorded. After gelation occurred, the gels were allowed to dry in a fume hood under ambient conditions to allow solvents to evaporate.

Physical Characterization of Synthesized Materials. The dried xerogel materials were ground into a fine powder using a ceramic mortar and pestle. IR spectra were taken of the synthesized solid xerogels through the use of a Nujol mull in which a small amount of the powder sample is mixed with the Nujol. The sample mull was pipetted between two KBr windows, which possessed a diameter of 25 mm and a thickness of 2 mm. A Nicolet Nexus 870 spectrophotometer scanned the range from 400 to 4000 cm^{-1} with a resolution of 2 cm^{-1} and a data spacing of 0.964 cm^{-1}. Fifty scans per sample were taken. The resulting spectra were further refined by the subtraction of the pure Nujol spectrum, taken under the same conditions, without scaling (scaling factor = 1). The sample chamber was thoroughly purged with dry, CO_2-free air prior to measurements in order to avoid the superposition of strong water and/or carbon dioxide bands onto the spectrum of interest.

XPS scans of powder samples were taken using a Surface Science Laboratories SSX-100 ESCA spectrometer using monochromatic Al Kα radiation (1486.6 eV). The system operated at a pass energy of 50 eV. Powder samples were housed in aluminum foil during analysis, and a flood gun was used at a voltage of 3 eV. The operating pressure of the vacuum chamber was less than 3×10^{-8} Torr. General scans covered the binding energy range of 0−1100 eV. Twenty high-resolution C 1s scans were run with a central binding energy (CBE) of 285 eV with a window width of 20 eV at a spot size of 400 μm. Twenty high-resolution scans were run on the Fe 2p region with a CBE of 715 eV, a window width of 30 eV at a spot size of 400 μm. Also, twenty high-resolution O 1s scans were run at a CBE of 532 eV using a spot size of 400 μm and a

(29) Duraes, L.; Costa, B. F. O.; Vasques, J.; Campos, J.; Portugal, A. *Mater. Lett.* **2005**, *59* (7), 859.
(30) Livage, J.; Henry, M.; Sanchez, C. *Prog. Solid State Chem.* **1988**, *18* (4), 259−341.
(31) Dobinson, B.; Hofmann, W.; Stark, B. P. *The Determination of Epoxides*; Pergamon Press: Oxford, 1969.

window width of 20 eV. Each high-resolution scan possessed a 0.1 eV per step interval. Curve fitting of the data was accomplished using the program Spectral Data Processor, Version 4.1.

XRD of the samples was performed on a Philips PW 1800 X-ray diffractometer. Patterns from 0° to 90° were examined with a step size of 0.02° using monochromatic Cu Kα X-rays with a wavelength of 1.54056 Å. Powder samples were analyzed using a zero background sample holder.

AFM images were taken using a Pacific Nanotechnology Nano-R AFM. Synthesized monoliths of the materials were placed on the surface of a wet epoxy, and the epoxy was allowed to dry. The sample was then embedded within the epoxy but left with an appreciable amount of the sample above the upper level of the epoxy, allowing access of the AFM probe to freely contact the sample surface. The sample was scanned using a scan size of 0.76 m × 0.76 μm at a scan rate of 1 Hz and a resolution of 512 scan lines. The AFM probes possess a radius of less than 10 nm with a force constant of 42 N/m. Transmission electron microscopy images were obtained from a Jeol JEM 100C TEM operating at 100 kV.

pH Studies of Gel Formation. A 0.43 M aqueous solution of Fe(III) was formed by adding 3.60 g of $Fe(NO_3)\cdot 9H_2O$ to 20 mL of deionized water.[27] To this solution, 77 mmol of respective gelation chemical was added and continually stirred. pH measurements were taken using a Fisher Scientific Accumet AB15 pH meter consisting of a glass pH indicating electrode in conjunction with a silver/silver chloride reference electrode starting with time zero corresponding to the addition of the gelation chemical (i.e., pyridine). A three-point calibration set at pH values of 4.0, 7.0, and 10.0 was performed on the pH meter prior to the onset of each experiment.

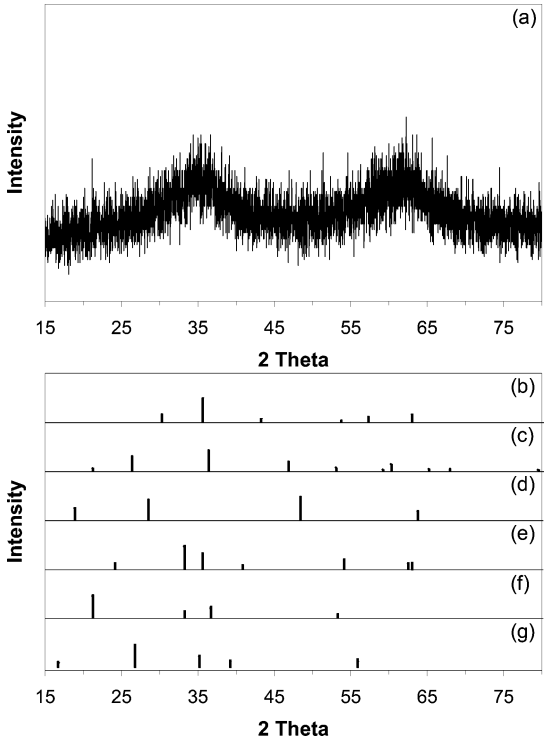

Figure 2. X-ray diffraction patterns for (a) $Fe^{(III)}_xO_yH_z$ xerogel formed with propylene oxide and X-ray diffraction patterns for various iron oxide/oxyhydroxide phases; (b) γ-Fe_2O_3; (c) $Fe(OH)_3$; (d) FeO(OH), ferrihydrite; (e) α-Fe_2O_3; (f) α-FeO(OH); and (g) β-FeO(OH).

Results and Discussion

Synthesis and Characterization of Iron(III) Oxide Xerogels. *Addition of Propylene Oxide as the Gelation Agent.* The addition of propylene oxide to a hydrated iron(III) nitrate metal salt precursor solution results in a heat-releasing reaction with the formation of a reddish-brown monolithic wet gel within 3 min. A dry, porous xerogel iron oxide matrix forms after the solvent in the gel is allowed to evaporate in ambient conditions. Figure 2a shows X-ray diffraction data for the as-synthesized sample. Due to its largely amorphous character as well as the fact that diffraction peaks tend to broaden in the nanoscale, the iron oxide material should be analyzed in a more qualitative manner. As a reference, Figure 2b−g shows the diffraction patterns for different iron(III) oxide, hydroxide, and oxyhydroxide phases: γ-Fe_2O_3; $Fe(OH)_3$; FeO(OH), ferrihydrite; α-Fe_2O_3; α-FeO(OH); and β-FeO(OH). The most intense peaks from many of these iron(III) phases fall within the two broad bands of the diffraction pattern in Figure 2a. However, while definitive identification of the iron species present in our sample is impossible, the XRD data give clear indication as to the nanocrytalline nature of the sample. Therefore, it would not be unreasonable to describe the material with the empirical formula of $Fe^{(III)}_xO_yH_z$. For the sake of simplicity, we will use to the term "iron oxide" to denote the formation of the mixture of iron(III) compounds that constitute the xerogel material.

XPS was utilized to evaluate the composition of the surface of the iron(III) oxide-based material synthesized from the weak base propylene oxide. Figure 3a shows the general survey spectrum of the material. Further analysis of the XPS spectrum was performed by high-resolution scans of the C(1s), Fe(2p), and O(1s) regions. Figure 3b shows the high-resolution C(1s) region after the data were adjusted to a C(1s) peak at 285.0 eV, as a result of differential charging of the insulating material shifting photoelectron lines to higher binding energies.[32] The C(1s) region can be deconvoluted into two separate peaks: (1) at a binding energy (BE) of 285.0 eV corresponding to aliphatic C−C bonding arising from the diol in eq 2 as well as residual ethanol and (2) the more electronegative C−O bond at a higher binding energy of 288.1 eV from the same diol. Important to note is the absence of an epoxide peak within the C(1s) high-resolution scan. This is due to the fact that propylene oxide is a key component in the reaction, and unlike a traditional catalyst, it actually gets consumed in the reaction.[27] The sample $Fe(2p_{3/2})$ peak is located at a binding energy of 711.4 eV, and the $Fe(2p_{1/2})$ peak is located at a BE of 725.8 eV, as shown in Figure 3, panels c and d. The corresponding $Fe(2p_{3/2})$ and $Fe(2p_{1/2})$ binding energy peaks of elemental iron are 710 and 723 eV, respectively. It is known that nonequivalent atoms of the same element in a solid give rise to peaks with different BE with increasing BE for increasing oxidation state.[33] This is demonstrated by the experimental values, and, along with the published values of the $Fe(2p_{3/2})$ peak for α-Fe_2O_3 corresponding to a BE of 711.6 eV, for FeO(OH) at a BE of 711.5 eV,[34] and the corresponding Fe_2O_3

(32) Schamm, S.; Berjoan, R.; Barathieu, P. *Mater. Sci. Eng. B* **2004**, *107* (1), 58.
(33) Briggs, D.; Seah, M. P. *Practical Surface Analysis*; John Wiley & Sons: Chicester, 1983; p 533.

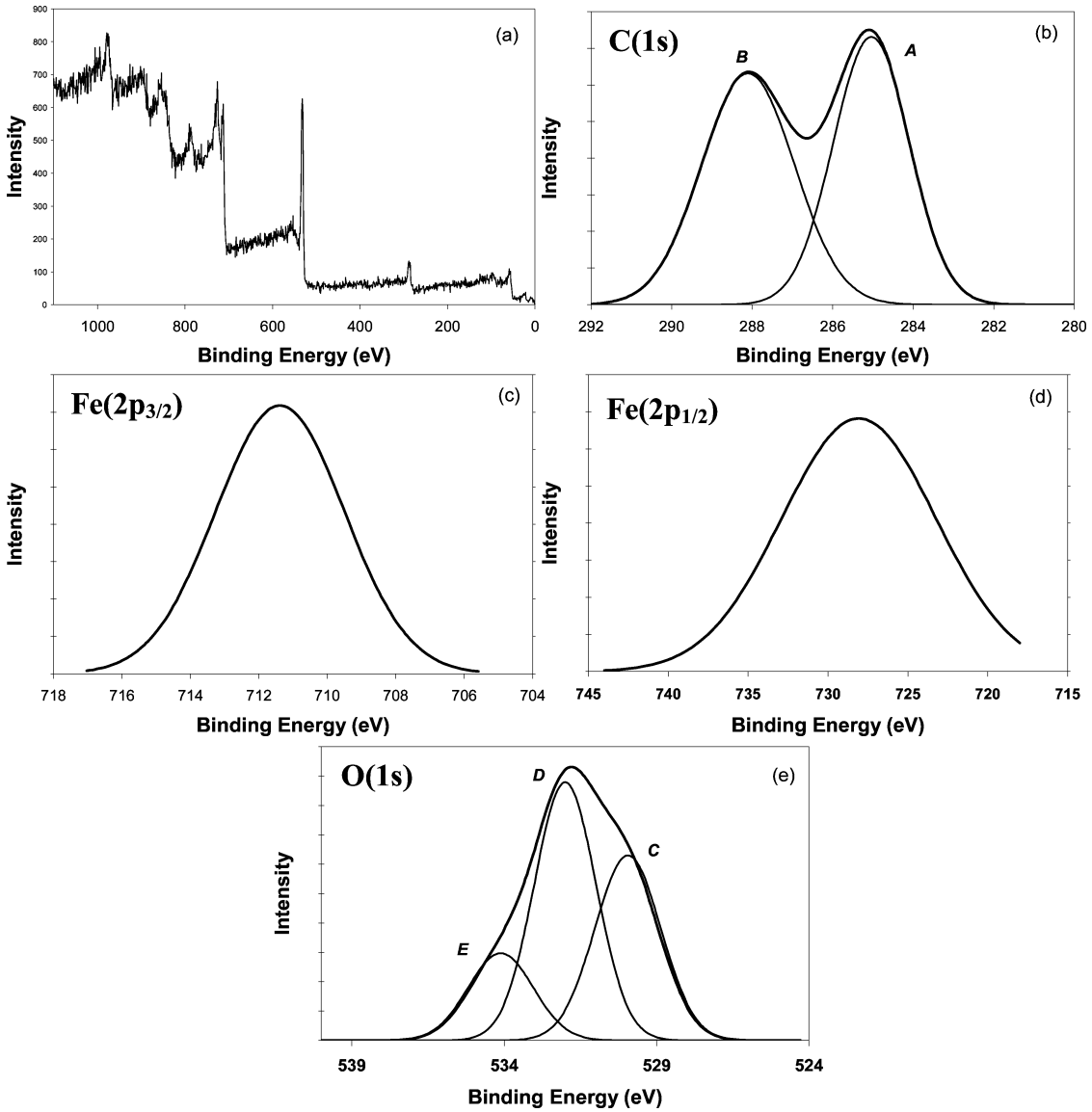

Figure 3. Photoemission spectra of a sol−gel synthesized iron(III) oxide/hydroxide from the weak base propylene oxide. (a) The general scan of the oxide material. (b) The high-resolution C 1s core level electrons and its deconvolution into three peaks. (c) The Fe $2p_{3/2}$ scan of the material, note the increase in binding energy of the peak from that of elemental iron, corresponding to an oxide material. (d) The Fe $2p_{1/2}$ scan of the material, again a higher binding energy peak in relation to that of elemental iron. (e) The O 1s core level emission spectrum.

$Fe(2p_{1/2})$ peak at a BE of 725.1, it can be concluded that the $Fe(2p_{1/2})$ and $Fe(2p_{3/2})$ peaks correspond to Fe(III).[35]

The O(1s) region can be deconvoluted into three peaks: 529.9 eV corresponding to the oxygen within α-Fe_2O_3; 531.9 eV corresponding to the oxygen within the iron hydroxyl compound FeO(OH), a product of the reaction of Fe_2O_3 with water as well as an intermediate in the proposed propylene oxide "proton scavenging" mechanism; and 534.0 eV corresponding to the oxygen−carbon bonding of the residual organic diol species from the synthesis as well as residual ethanol.[36] The relative ratios between the three experimental O(1s) peaks corresponding to Fe_2O_3, FeO(OH), and O−C are 37.1, 47.1, and 16.8, respectively. This indicates that the majority of the synthesized product (~84.2%) is an iron oxide or iron hydroxide material, with the balance of the sample oxygen originating from residual organic species. The reported O(1s) peak location for α-Fe_2O_3 is 529.9 eV, which is the value reported in the synthesized material here, whereas the O(1s) peak of elemental oxygen is centered at 532.0 eV, again proving the existence of an iron(III) material,[35] supporting an empirical formula of $Fe^{(III)}{}_xO_yH_z$. The O(1s) region is shown in Figure 3e. The XPS data for propylene oxide as the gelation agent are summarized in Table 1.

AFM imaging displays surface topography of a porous material comprised of clusters that are roughly 25 nm in diameter with a pore size of approximately 5 nm, and TEM images reveal individual particles within each cluster of 2−5 nm, as shown in Figure 4a,b.

Addition of Pyridine as the Gelation Agent. The addition of pyridine to an equivalent hydrated iron nitrate solution results in the formation of a dark-brown material after 10

(34) Tan, B. J.; Klabunde, K. J.; Sherwood, P. M. A. *Chem. Mater.* **1990**, *2*, 186−191.
(35) Mills, P.; Sullivan, J. L. *J. Phys. D: Appl. Phys.* **1983**, *16*, 723−732.
(36) Tannenbaum, R.; Hakanson, C.; Zeno, A. D.; Tirrell, M. *Langmuir* **2002**, *18* (14), 5592−5599.

Table 1. Binding Energies, FWHM Values, Percentage of Total Peak Area, and Assignment of Atoms of the XPS of the O(1s) and C(1s) Core Electron Regions for a Sol−Gel Synthesized Iron(III) Oxide/Hydroxide from Propylene Oxide Corresponding to Figure 3

peak label	BE (eV)	FWHM (eV)	% of total area	assignment of atoms
		C 1s		
A	285.0	2.26	50.7	aliphatic
B	288.1	2.20	49.3	**C**−O
		O 1s		
C	529.9	2.55	36.1	Fe_2**O**$_3$
D	531.9	2.38	47.1	FeO(**O**H)
E	532.0	2.51	16.8	**O**−C

days. Ambient drying of the material for an excess of 2 weeks yields a dry xerogel. Figure 5 shows the structure of the material having a porous morphology with individual, interconnected $Fe^{(III)}_xO_yH_z$ clusters on the order of 40−50 nm with individual particles of approximately 10 nm.

The survey XPS spectrum of the newly synthesized material in Figure 6a clearly shows the C(1s), O(1s), Fe($2p_{3/2}$), Fe($2p_{1/2}$), and N(1s) peaks. High-resolution scans of the C(1s) peak, seen in Figure 6b, show the deconvolution of five distinct peaks. The peak at 285.0 eV corresponds to

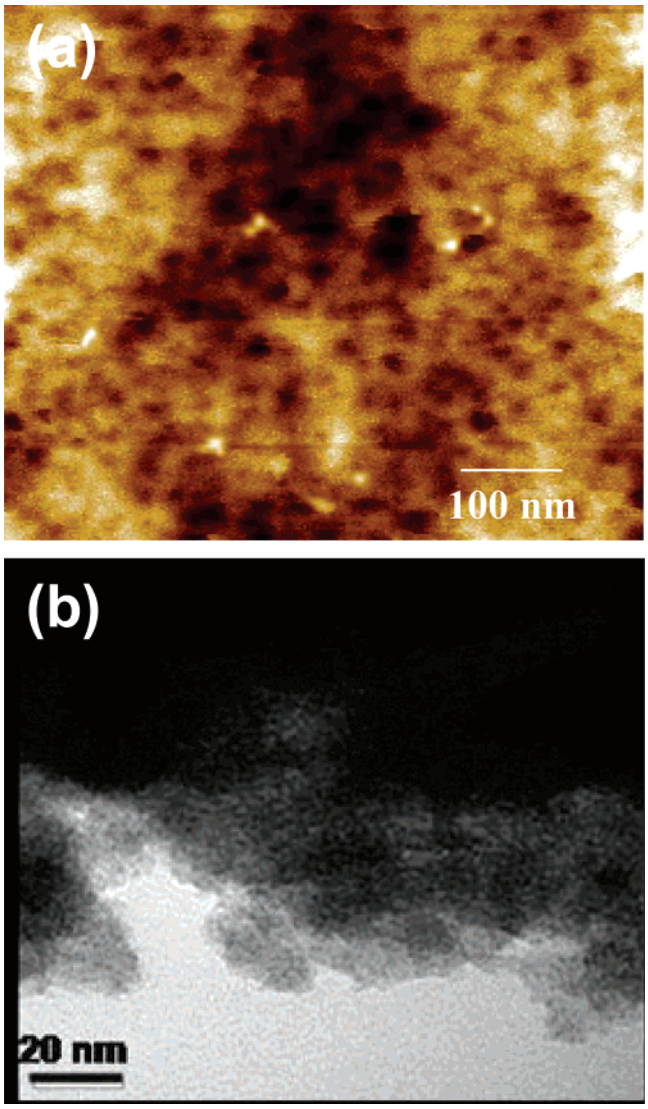

Figure 4. Imaging of nanoscale $Fe^{(III)}_xO_yH_z$ xerogel using propylene oxide as gelation agent by (a) AFM and (b) TEM.

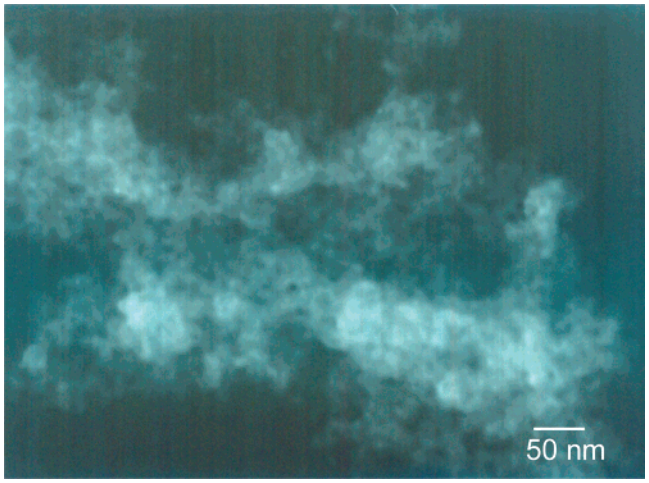

Figure 5. Imaging of nanoscale $Fe^{(III)}_xO_yH_z$ xerogel using pyridine as gelation agent from a ferric nitrate nonahydrate/ethanol sol.

the double-bonded carbon within the pyridine molecule, 286.5 eV corresponds to the remaining aliphatic bonds arising from the ethanol solvent as well as single-bonded carbon−carbon bonds remaining from the pyridine molecule, 287.7 eV corresponds to the C−N═C bond of the pyridine molecule, 289.0 eV corresponds to the C−N^+═C bond, which arises from the possible protonation of the pyridine molecule during the sol to gel reaction, and 290.3 eV corresponds to the C−OH alcohol bonding of residual ethanol. The proposed C−N^+═C bond as well as examination of the N(1s) peak will be discussed within the section on pH studies of gel formation. High-resolution scans of the Fe($2p_{3/2}$) and Fe($2p_{1/2}$) peaks are shown in Figure 6, panels c and d. The Fe($2p_{3/2}$) peak appears at a binding energy of 711.1 eV, and the Fe($2p_{1/2}$) peak appears at a BE of 725.1 eV. This gives a Fe($2p_{1/2}$) to Fe($2p_{3/2}$) peak maximum to peak maximum difference of 14.0 eV, significantly larger than the same peak to peak difference for elemental Fe of 13.2 eV and similar to that of Fe_2O_3, which has a similar reported difference of 13.6 eV.[37] As with the sample synthesized from the addition of propylene oxide, the material obtained from the addition of pyridine as the gelation agent exhibits a chemical shift to higher binding energies for the Fe(2p) peaks, which is indicative of the formation of an iron(III) oxide/hydroxide material.

High-resolution scans of the O(1s) peak are shown in Figure 6(e). The peak can be deconvoluted into three distinct peaks: 530.1 eV corresponding to the oxygen within the iron(III) oxide material, 532.5 eV corresponding to the oxygen within the iron hydroxyl compound FeO(OH), a product of the reaction of Fe_2O_3 with water, and 534.8 eV corresponding to the O−C corresponding to the oxygen bonding within residual organic species from the ethanol.[38] The relative peak ratios for the oxygen corresponding to Fe_2O_3, FeO(OH), and O−C are 51.5, 35.9, and 12.5, respectively. Again, in the case of pyridine being used as the weak base gelation chemical, there is a large (87.5%)

(37) Wagner, C. D.; Riggs, W. M.; Davis, L. E.; Moulder, J. F. *Handbook of X-ray Photoelectron Spectroscopy*, 1st ed.; Perkin-Elmer Corporation (Physical Electronics): 1979.
(38) Richter, M.; Abramova, A.; Bentrup, U.; Fricke, R. *J. Appl. Spectros.* **2004**, *71* (3), 400−403.

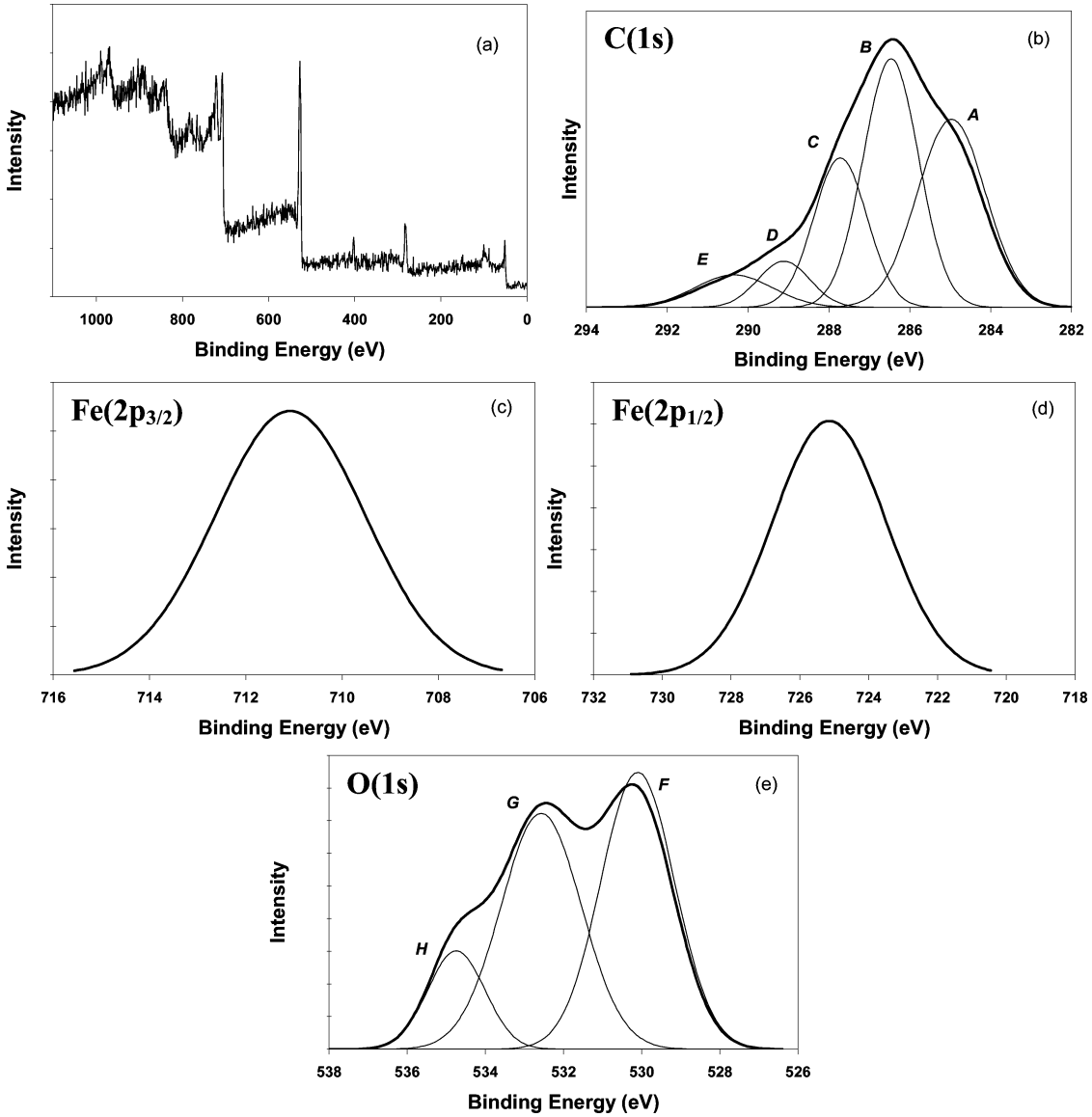

Figure 6. The photoemission spectra of a sol−gel synthesized iron(III) oxide/hydroxide from the weak base pyridine. (a) The general scan of the oxide material. (b) The high-resolution C 1s core level electrons and its deconvolution into five peaks. (c) The Fe $2p_{3/2}$ scan of the material, note the increase in binding energy of the peak from that of elemental iron, corresponding to an iron(III) oxide material. (d) The Fe $2p_{1/2}$ scan of the material, again a higher binding energy peak in relation to that of elemental iron. (e) The O 1s core level emission spectrum, deconvoluted into three distinct peaks.

Table 2. Binding Energies, FWHM Values, Percentage of Total Peak Area, and Assignment of Atoms of the XPS of the O(1s) and C(1s) Core Electron Regions for a Sol−Gel Synthesized Iron(III) Oxide/ Hydroxide from the Weak Base Pyridine Corresponding to Figure 6

peak label	BE (eV)	FWHM (eV)	% of total area	assignment of atoms
		C 1s		
A	285.0	1.58	20.9	**C**═C
B	286.5	1.77	48.1	**C**−C
C	287.7	1.62	23.6	**C**−N═C
D	289.0	1.26	5.2	**C**−N^+═C
E	290.3	1.18	2.2	**C**−O
		O 1s		
F	530.1	2.48	51.5	Fe_2**O_3**
G	532.5	2.07	35.9	FeO(**O**H)
H	534.8	1.69	12.5	**O**−C

presence of iron oxide/hydroxide product in the material with the balance corresponding to residual solvents. The XPS data for pyridine as the gelation agent is summarized in Table 2.

Addition of Tetrahydrofuran as the Gelation Agent. The addition of tetrahydrofuran to the same iron nitrate solution results in the formation of a gel in 7 days. Ambient drying of the wet gel for an excess of 2 weeks yields a dry xerogel. Figure 7 shows TEM image revealing a porous structure with $Fe^{(III)}_xO_yH_z$ particles of approximately 5 nm forming clusters of 25 nm.

An XPS survey spectrum of the material is shown in Figure 8a. Figure 8b shows the C(1s) high-resolution scan can be deconvoluted into two peaks. The peak at a BE of 285.0 eV corresponds to the C−C bonding of the residual organic species from the ethanol solvent as well as the aliphatic bonding within the diol product of the reaction mechanism, and the peak at 288.8 can be attributed to the residual C−O bonding from residual ethanol as well as from the diol mechanism product. High-resolution Fe($2p_{3/2}$) and Fe($2p_{1/2}$) scans are shown in Figure 8, panels c and d, respectively. The Fe($2p_{3/2}$) peak appears at a BE of 710.7 eV, and the Fe($2p_{1/2}$) peak is found at a BE of 724.7, resulting in a peak to peak distance of 14.0 eV. This is similar to the sample synthesized using propylene oxide. From the Fe(2p)

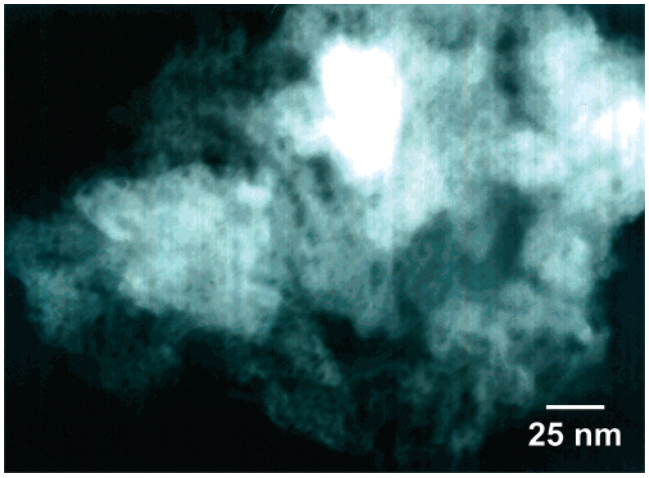

Figure 7. Imaging of nanoscale $Fe^{(III)}{}_xO_yH_z$ xerogel using THF as gelation agent from a ferric nitrate nonahydrate/ethanol sol.

peaks, the higher binding energies than elemental Fe confirm the existence of an Fe(III) material. A high-resolution O(1s) scan is shown in Figure 8e. The peak at a BE of 529.7 corresponds to the oxygen bonding within Fe_2O_3, the peak at 531.3 eV corresponds to the oxygen within the iron hydroxyl compound FeO(OH), and the peak at 532.5 eV corresponds to the O−C bonding from the residual solvents. The relative peak area ratios of the Fe_2O_3, FeO(OH), and O−C peaks are 44.1, 33.5, and 22.4, respectively. The XPS data for tetrahydrofuran as the gelation agent are summarized in Table 3.

A general note on all three synthesized samples is that while the majority of the oxygen within the sample originates from an iron oxide or hydroxyl material, drying the samples under ambient conditions permits a substantial percentage of residual organic species to remain in the final material. Given the intended use of these materials in highly exothermic reactions with potential inclusion in projectile casing, residual organic materials in the nanonetwork matrix may prove important in the overall energetic efficiency of the oxidative/reductive process. Table 4 summarizes the XPS

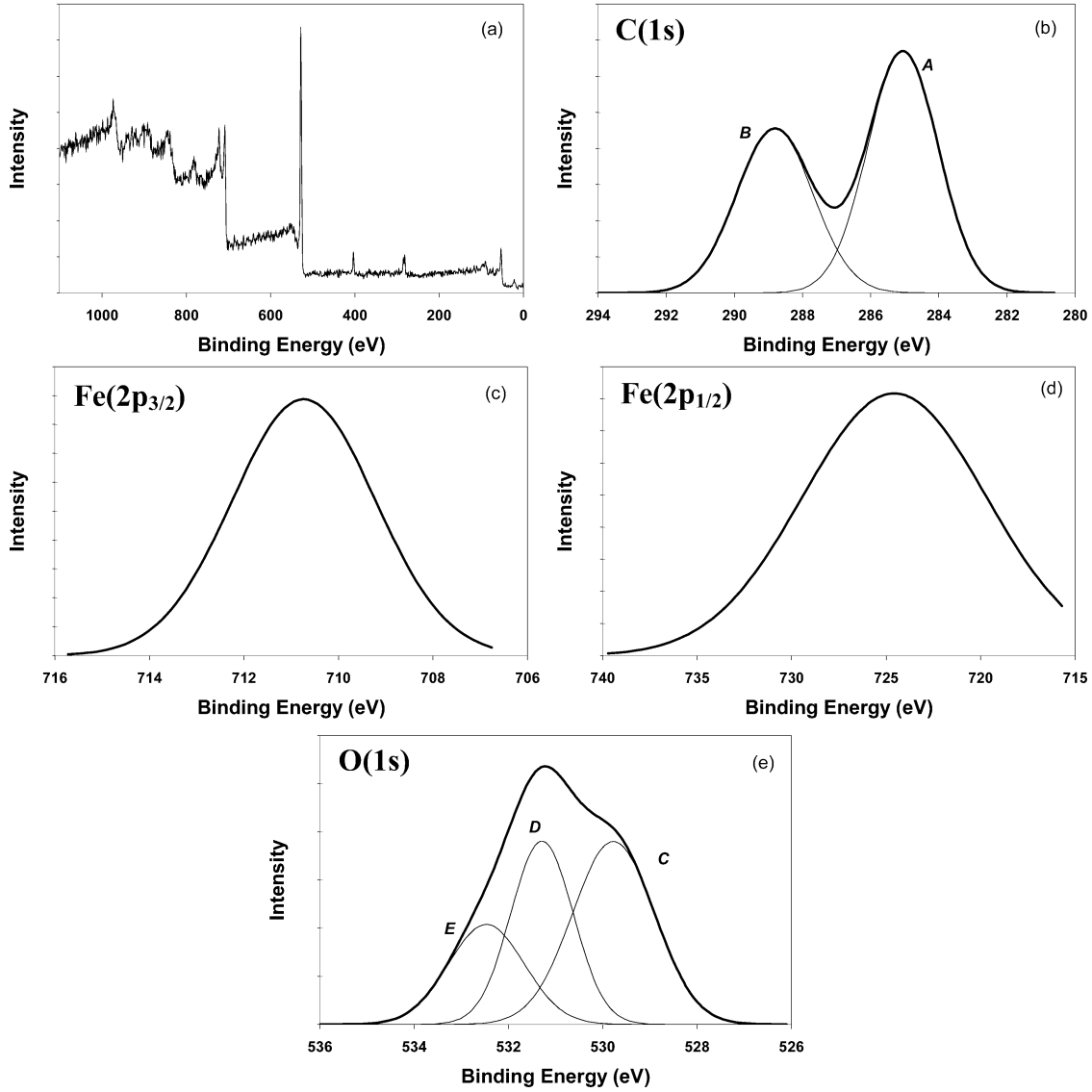

Figure 8. Photoemission spectra of a sol−gel synthesized iron(III) oxide/hydroxide from the weak base epoxide, tetrahydrofuran. (a) The general scan of the oxide material. (b) The high-resolution C 1s core level electrons and its deconvolution into two peaks. (c) The Fe $2p_{3/2}$ scan of the material, note the increase in binding energy of the peak from that of elemental iron, corresponding to an iron(III) oxide material. (d) The Fe $2p_{1/2}$ scan of the material, also a higher binding energy peak in relation to that of elemental iron. (e) The O 1s core level emission spectrum, deconvoluted into three distinct peaks. Note the similarities in photoemission spectra with those of Figure 4, the iron(III) oxide material synthesized from a 1,2-epoxide, propylene oxide.

Table 3. Binding Energies, FWHM Values, Percentage of Total Peak Area, and Assignment of Atoms of the X-ray Photoemission Spectrum (XPS) of the O(1s) and C(1s) Core Electron Regions for a Sol−Gel Synthesized Iron(III) Oxide/Hydroxide from the Epoxide Tetrahydrofuran Corresponding to Figure 8

peak label	BE (eV)	FWHM (eV)	% of total area	assignment of atoms
		C 1s		
A	285.0	2.64	42.4	aliphatic
B	288.8	2.44	57.6	**C**−O
		O 1s		
C	529.7	2.05	44.1	Fe_2**O_3**
D	531.3	1.55	33.5	FeO(**O**H)
E	532.5	1.90	22.3	**O**−C

Table 4. Summary of Binding Energies (eV) of the XPS in Formation of $Fe^{III}_xO_yH_z$ Xerogels for the Three Systems Presented for Fe($2p_{3/2}$), Fe($2p_{1/2}$), and O(1s)

			O 1s		
sample	Fe($2p_{3/2}$)	Fe($2p_{1/2}$)	Fe_2**O_3**	FeO(**O**H)	**O**−C
propylene oxide	711.4	725.8	529.9	531.9	532.0
pyridine	711.1	725.1	530.1	532.5	534.8
THF	710.7	724.7	529.7	531.3	532.5

binding energies of the Fe($2p_{1/2}$), Fe($2p_{3/2}$), and O(1s) photoelectron binding energy peaks for the three samples, showing very similar results for all three gelation systems.

Mechanistic Studies of Gel Formation. The pH of the reacting solution using propylene oxide as the gelation agent has been shown to increase with time. This is explained due to the addition of a base to an acidic precursor solution and disappearance of the hydronium ions from solution as they recombine with the anions from the original salt (i.e., nitrate ions). In order to study the mechanism of the gelation processes using propylene oxide, pyridine, and tetrahydrofuran as gelation agents, pH data were collected for all three reactions. Figure 9 shows the pH profile of the three systems as a function of reaction time. Clearly, there is an increase in reaction pH with time for each of the three systems. This supports the hypothesis shown in eqs 2 and 3, where the weak base reacts with the hydrated metal complex producing a protonated conjugated weak acid molecule resulting in further release of hydronium ions into solution.

From the pH studies and the previously hypothesized mechanism involving propylene oxide, we propose the following reaction mechanisms for the sol−gel reactions involving the weak base gelation agents pyridine and tetrahydrofuran. In the case of pyridine as the gelation agent, a pyridine molecule is capable of extracting a proton from the water molecules in the coordination sphere of the hydrated iron cation to form a pyridinium ion, as shown in eq 4. The proton scavenging cascade will subsequently lead to the formation of Fe_2O_3.

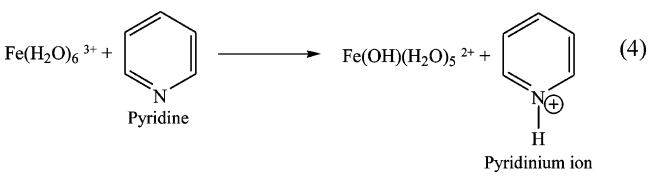

(4)

When propylene oxide is used as the gelation agent, the protonated epoxide undergoes an irreversible ring-opening reaction due to the high strain energy associated with the three-membered ring. In the case of pyridine, the pyridinium ion is a six-membered ring with aromatic character, which is highly stable and has low associated ring strain. Therefore, whereas with the systems involving propylene oxide and THF, XPS results demonstrate the existence of a diol species, which is the result of the ring-opening reaction, the pyridinium ion is relatively stable, especially in the presence of the anionic species present in the system.

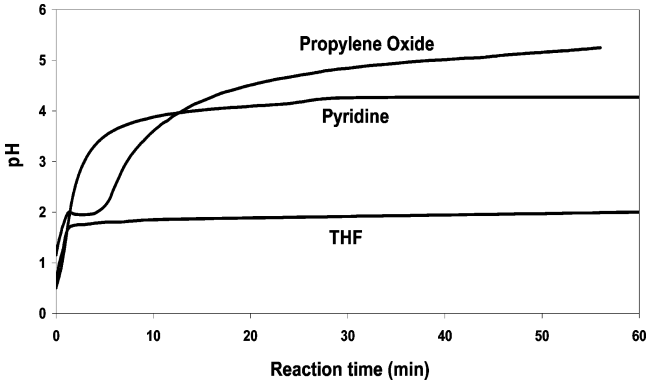

Figure 9. pH profile of reaction study of gels formed using propylene oxide, pyridine, and THF as gelation agents. Notice the increase in pH with increasing reaction time for all three systems.

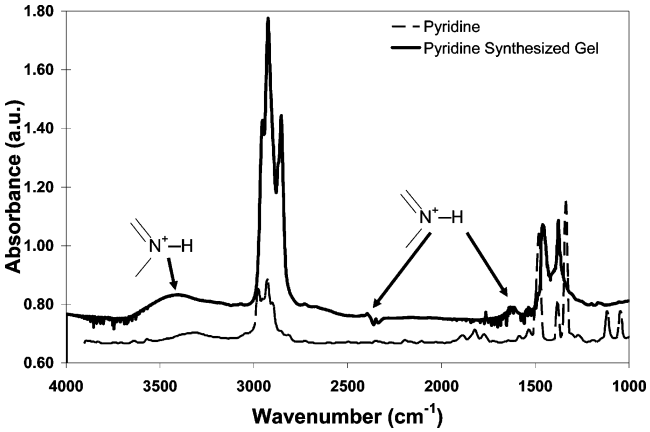

Figure 10. IR spectrum displaying presence of N^+−H bond at 3428, 2380, and 1630 cm^{-1} involved in the mechanism of formation of iron oxide xerogel from pyridine as the gelation agent.

Additional evidence of the proposed mechanism in the formation of the pyridinium ion is demonstrated by FTIR spectroscopy. Figure 10 shows an FTIR spectrum of a $Fe^{(III)}_xO_yH_z$ xerogel synthesized using pyridine as the gelation agent. In contrast to pure pyridine, a peak at 3428 cm^{-1} from the gel material corresponds to the asymmetric stretching vibration of the quaternary protonated amine bond present in the pyridinium ion as a result of the proton extraction from the coordinated water molecules.[39] This is echoed by the corresponding symmetric stretching vibration at ∼2380 cm^{-1} and the in-plane deformation vibrations of the pyridinium internal modes at ∼1630 cm^{-1}.[40−43] It is important

(39) Tannenbaum, R.; Rutkowska, M.; Eisenberg, A. *J. Polym. Sci.* **1987**, *25*, 663−671.
(40) Cummings, D. L.; Wood, J. L. *J. Mol. Struct.* **1973**, *17* (2), 257−264.
(41) Florian, J.; Kubelkova, L.; Kotrla, J. *J. Mol. Struct.* **1995**, *349*, 435−438.
(42) Glazunov, V. P.; Odinokov, S. E. *Spectrochim. Acta, Part A* **1982**, *38* (4), 399−408.
(43) Harmon, K. M.; Shaw, K. E. *J. Mol. Struct.* **1999**, *513* (1−3), 219−230.

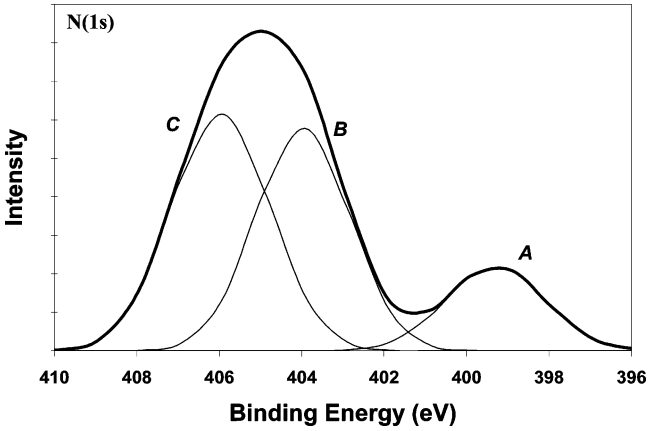

Figure 11. N 1s photoemission spectrum of a sol−gel synthesized material using the weak base pyridine. The region is deconvoluted into three peaks corresponding to the C−N bonding representative of pyridine and the $C-N^+$ bonding representative of a pyridinium ion as well as an N−O peak.

Table 5. Binding Energies, FWHM Values, Percentage of Total Peak Area, and Assignment of Atoms of the XPS of the N(1s) Core Electron Region for a Sol−Gel Synthesized Iron(III) Oxide/Hydroxide from the Epoxide Pyridine Corresponding to Figure 11

peak label	BE (eV)	FWHM (eV)	% of total area	assignment of atoms
		N1s		
A	399.0	1.74	13.4	**N**−C
B	403.9	2.01	39.8	$\mathbf{N}^+$−C
C	405.9	2.64	46.8	**N**−O

to note that the FTIR characterization of the xerogel powder was performed using the Nujol mull sample preparation technique; hence, the spectrum shown is a result of the subtraction of pure Nujol (a heavy paraffin oil with a relatively uncomplicated infrared spectrum, with major peaks between 2950−2800, 1465−1450, and 1380−1370 cm^{-1}) from the raw spectrum of the sample. This ensured that the spectrum of the pyridinium moiety could be presented without being obscured by the Nujol reference.

Further evidence of this proposed mechanism and the existence of the pyridinium ion is seen in the high-resolution XPS scans of the N(1s) region of the material synthesized in the presence of the pyridine as the gelation agent, shown in Figure 11. Three peaks are deconvoluted from the high-resolution spectrum: One peak at 399.0 eV corresponding to the C−N═C bonding arising from the aromatic pyridine molecule; a second peak at 403.9 eV corresponding to the $C-N^+$═C aromatic bonding representative of the pyridinium ion, as protonated forms of N atoms in pyridine are shifted to higher binding energies;[44] and a third peak at 405.9 eV, corresponding to the N−O bond originating from the remaining nitrate anions originating in the initial iron nitrate precursor. Table 5 summarizes this data.

(44) Ada, E. T.; Hanley, L.; Etchin, S.; MeIngailis, J.; Dressick, W. J.; Mu-San, C.; Calvert, J. *J. Vac. Sci. Technol. B* **1995**, *13* (6), 2189−2196.

The material synthesized using the epoxide THF as the gelation agent seems to follow a similar reaction mechanism as that of propylene oxide. The THF molecule is capable of extracting a proton from the coordination sphere of a hydrated iron complex, producing a protonated 1,4-epoxide and the hydroxo ligand, $Fe(OH)(H_2O)_5^{2+}$ Then, a nucleophile can attack the protonated 1,4-epoxide molecule in an irreversible ring-opening reaction creating a protonated diol, which can deprotonate and form a diol as well as extract hydronium ions into solution, as shown in eqs 5 and 6.

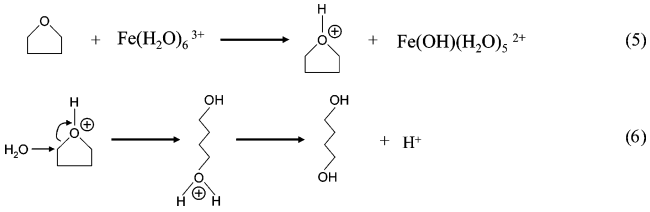

Conclusions

The intent of the work presented in this paper was to study and expand upon the published theory of the sol−gel synthesis of iron(III) oxide/hydroxide materials characterized by the addition of a weak base epoxide, propylene oxide, to an iron nitrate solution. In addition to synthesizing new materials from other weak bases, reaction mechanisms have been proposed stemming from a proton scavenging mechanism. Two epoxides (propylene oxide and tetrahydrofuran) and a heterocyclic nitrogen compound (pyridine) have been successfully used in the synthesis of porous iron(III) oxide-based materials. XPS, XRD, IR spectroscopy, TEM, and AFM have been used to characterize the new materials. Detailed analysis of XPS data has revealed the formation of an iron(III) oxide/hydroxide in each of the three individual syntheses. TEM and AFM images show a naturally porous surface structure with individual nanoscale $Fe^{(III)}_xO_yH_z$ clusters. The broadening of peaks in the XRD pattern was also consistent with the nanocrystalline nature of the particles that were formed. Mechanistically, the proton scavenging mechanism is indeed relevant for all three syntheses. The epoxides (i.e., propylene oxide and tetrahydrofuran) scavenge protons from the hydrated iron complexes to form protonated epoxides, which are then irreversibly ring-opened to form diols. Pyridine also reacts with the hydrated iron complexes, extracting protons, to form the protonated pyridinium ion. Reaction mechanisms were confirmed by pH and IR spectroscopy data.

Acknowledgment. This work was supported by the Air Force/Bolling AFB/DC MURI project on Energetic Structural Materials (Award F49620-02-1-0382). The authors are indebted to Professors Sathya Hanagud and Naresh Thadhani of the Georgia Institute of Technology, Al Steigman of Florida State University, and Dr. Alex Gash of Lawrence Livermore Labs for their participation in rewarding scientific interactions.

CM0609101